A study of the ground state of manganese dimer using quasidegenerate perturbation theory

Shigeyoshi Yamamoto[a)]
Faculty of Liberal Arts, Chukyo University, 101-2 Yagoto-Honmachi, Showa-ku, Nagoya, Aichi 466-8666, Japan

Hiroshi Tatewaki and Hiroko Moriyama
Graduate School of Natural Sciences, Nagoya City University, 1 Yamanohata, Mizuho-cho, Mizuho-ku, Nagoya, Aichi 467-8501, Japan

Haruyuki Nakano
Department of Chemistry, Graduate School of Sciences, Kyushu University, 6-10-1 Hakozaki, Higashi-ku, Fukuoka 812-8581, Japan

(Received 9 December 2005; accepted 27 January 2006; published online 23 March 2006)

We study the electronic structure of the ground state of the manganese dimer using the state-averaged complete active space self-consistent field method, followed by second-order quasidegenerate perturbation theory. Overall potential energy curves are calculated for the $^1\Sigma_g^+$, $^{11}\Sigma_u^+$, and $^{11}\Pi_u$ states, which are candidates for the ground state. Of these states, the $^1\Sigma_g^+$ state has the lowest energy and we therefore identify it as the ground state. We find values of 3.29 Å, 0.14 eV, and 53.46 cm^{-1} for the bond length, dissociation energy, and vibrational frequency, in good agreement with the observed values of 3.4 Å, 0.1 eV, and 68.1 cm^{-1} in rare-gas matrices. These values show that the manganese dimer is a van der Waals molecule with antiferromagnetic coupling. © *2006 American Institute of Physics*. [DOI: 10.1063/1.2178798]

I. INTRODUCTION

Transition metal dimers are starting points for studying the fundamental properties of transition metal clusters. However, for some dimers it is difficult to calculate even the bond length theoretically. For instance, obtaining a potential energy curve of Cr_2 suitable for comparison with experiment exceeds the capabilities of the Hartree-Fock and complete active space self-consistent field (CASSCF) methods.[1] It is necessary to calculate at the level of the multiconfigurational second-order perturbation theory with a CASSCF reference function[2,3] (CASPT2) or use the multireference configuration interaction singles and doubles[4] (MRCISD) method. As well as Cr_2, the Mn dimer is also a challenging molecular system for theoretical study.

Mn displays an antiferromagnetic character in bulk states, but behaves differently in cluster states. Specifically, Mn_4, and Mn_5 were suggested to be ferromagnetic by experiments.[5,6] However, the dimer has the singlet ground state, as indicated by resonance Raman spectra[7,8] in rare-gas matrices. Thus the dimer has antiferromagnetic character. The resonance Raman experiments determined the bond length to be 3.4 Å. An electron spin resonance (ESR) experiment[6] also supports the singlet ground state and found -9 ± 3 cm^{-1} for the Heisenberg effective exchange integral J. Kant *et al.*[9] accounted for the dissociation energy as 0.1 eV. A comprehensive review has been made by Lombardi and Davis[10] for experimental research on transition metal dimers and clusters.

Extensive theoretical studies have been performed to clarify the anomalous character of Mn_2. Nesbet[11] stated in 1964 that the bond length of the Mn dimer is 2.88 Å and that it is antiferromagnetic on the basis of approximate Hartree-Fock calculations. He suggested that the ground state of the Mn dimer is singlet. The J value was calculated to be -4.1 cm^{-1}.

A number of studies[12–22] based on density functional theory (DFT) followed. Many results have been presented from DFT calculations, but even fundamental properties such as bond length differ from one another. For example, Nayak and Jena[14] performed DFT calculations with several functionals (LSDA, BPW94, B3LYP) and gave 1.62, 2.50, and 3.55 Å as the bond lengths. These values are so different that no reliable bond length can be quoted. The spin multiplicity of the ground state also depends on the functional used, being 3, 11, and 11.

Yanagisawa *et al.*,[18] Barden *et al.*,[19] and Gutsev *et al.*[20] performed a series of DFT calculations on the first-row transition metal dimers. These research groups used various functionals, but they did not reach the same conclusion. Yanagisawa *et al.*[18] suggested that the Mn dimer is unbound. Barden *et al.*[19] investigated several states ($^1\Sigma_g^+$, $^{11}\Sigma_u^+$, $^{11}\Pi_u$, $^{11}\Sigma_g^+$) as candidates for the ground state, but were prudent in drawing a conclusion. They pointed out that DFT would not be a good choice for investigation of the Mn dimer. Gutsev *et al.*[20] reported that the $^{11}\Pi_u$ state is the ground state.

We now survey previous studies performed with *ab initio* molecular orbital (MO) methods. Calculations using second-order Møller-Plesset perturbation theory (MP2) with

a)Author to whom correspondence should be addressed. Fax: +81-52-835-7183. Electronic mail: syamamot@lets.chukyo-u.ac.jp

the Hartree-Fock MOs in Ref. 18 did not yield a bound ground state. The CASSCF potential energy curve[23] was also unbound. Wang and Chen[24] recently performed CASPT2 (Ref. 25) calculations with an effective core potential on the Mn dimer and obtained a singlet ground state with a bond length of 3.64 Å. This is in good agreement with experiment. However, they present potential energy curves only for the long nuclear distance region (R=3.0–4.4 Å), and the spatial symmetry is not assigned for each spin state calculated. More extensive investigations are needed, based on the overall potential energy curve.

We aim in this study to calculate properties accurately so that they can be compared with experiment. We calculate the potential energy curves using cutting-edge *ab initio* MO methods. We then discuss the bonding mechanism in the Mn dimer. As described by Bauschlicher,[23] in the $^1\Sigma_g^+$ CASSCF wave function more than 100 electronic configurations mix each other with small weight. It is necessary to use a method which can treat a large number of reference configurations equally.

The MRCISD method has high computational cost, because it must treat one- and two-electron excited configurations from reference configurations exceeding 100. Also, the configuration interaction (CI) method is not generally very efficient in accounting for electronic correlation effects. We therefore use second-order multiconfiguration quasidegenerate perturbation theory (MCQDPT2).[26] This method is efficient in accounting for the electronic correlation effects in the CAS wave function.

The ground state of the manganese atom is the ^6S state of the $(4s)^2(3d)^5$ configuration. The first excited state is the ^6D state of the $(4s)^1(3d)^6$ configuration. It is expected that the bond of the Mn dimer can be described by the combination of these two configurations. As the nuclear distance decreases starting from the two atomic states, the ground state can be roughly represented by (^6S+^6S), (^6S+^6D), and (^6D+^6D). However, there are peculiar circumstances for Mn. Since the Mn atom has a promotion energy[27] [the one-electron transfer energy from $(4s)^2(3d)^5$ to $(4s)^1(3d)^6$] of 2.14 eV, which is exceptionally high compared with other transition metal atoms, hybridization between the 4*s* and 3*d* atomic orbitals (AOs) would not emerge in the Mn dimer. Accordingly, covalent bonds will not be formed and the outermost four electrons will occupy the bonding and antibonding MOs consisting of the 4*s* AOs. The 3*d* electrons will not take part in bond formation, and overall a weak bond will be formed by the attractive van der Waals force. An atomiclike configuration of $((4s)^2(3d)^5{}^6S+(4s)^2(3d)^5{}^6S)$ is therefore expected near the equilibrium bond length (3.4 Å).

In summary, the bonds in the first-row transition metal dimers can in general be described by a combination of $(4s)^2(3d)^{n-2}$ and $(4s)^1(3d)^{n-1}$. This model is employed in the studies of Sc_2 and Ti_2 by Suzuki *et al.*[28,29] In the present study we shall elucidate the electronic structure of the Mn dimer, based on this model.

II. COMPUTATIONAL DETAILS

A. Basis set

We constructed a basis set from the Gaussian-type functions (18*s*12*p*8*d*) developed by Koga *et al.*[30] We augmented this set with three *p*-type primitive functions, developed by Tatewaki *et al.*[31] to describe the valence 4*p* AOs. Using these primitive functions, we expanded 3*s* and 3*p* as double zeta, 4*s* and 4*p* as triple zeta, and 3*d* as quadruple zeta. We also added the 4*f*2*g* polarization functions developed by Sekiya *et al.*[32] and contracted the entire set as (18*s*15*p*8*d*4*f*2*g*)/[7*s*6*p*4*d*4*f*2*g*]. This basis set was used in the form of spherical harmonic functions. The exponents and expansion coefficients are listed in Table I.

The 12 MOs composed mainly of the 4*s* and 3*d* AOs are chosen to construct the CAS. All computation was done using the GAMESS program.[33]

B. Spin multiplicity and spatial symmetry

The molecular symmetry of the Mn dimer is $D_{\infty h}$, but because the GAMESS program supports only Abelian point groups, we performed the calculations under D_{2h} symmetry. We investigate three states ($^1\Sigma_g^+$, $^{11}\Sigma_u^+$, $^{11}\Pi_u$) which have been considered as the most promising candidates for the ground state from the *ab initio* MO (Refs. 11 and 23) and DFT (Refs. 19 and 20) studies so far.

We solve the $^1\Sigma_g^+$ state as the ^1A_g state of D_{2h}, where $^1\Sigma_g^+$ and $^1\Delta_g$ coexist. In fact, the ^1A_g excited state arose as a Δ state mainly from $(4s_\sigma)\rightarrow(3d_{\delta x2-y2})$ and $(4s_d^*)\rightarrow(3d_{\delta x2-y2}^*)$ excitations. The $^{11}\Sigma_u^+$ state is solved as the $^{11}B_{1u}$ state. The $^{11}\Pi_u$ state is solved as an average of the $^{11}B_{3u}$ and $^{11}B_{2u}$ states. The purpose of averaging the two states of different irreps is to make the MOs symmetry adapted with respect to x and y. The z coordinate runs along the Mn–Mn axis. To perform CASSCF calculations averaged between two states of different irreps, we used the Ames Laboratory determinant full-CI code, written by Ivanic and Ruedenberg, which is implemented in the GAMESS program. All other calculations were done in configuration state function (CSF) basis.

C. The problem of multiple solutions

In the region of long nuclear distance, the electronic configuration can be represented by $(4s)^2(3d)^5$ for each atom, and in the short distance region by $(4s)^1(3d)^6$. If one performs standard CASSCF calculations for the $^1\Sigma_g^+$ state in the middle bond length region, one may obtain two sets of solutions having characteristics of $((4s)^2(3d)^5+(4s)^2(3d)^5)$ and of $((4s)^1(3d)^6+(4s)^1(3d)^6)$, which are, respectively, obtained from the outer and inner regions. These two sets have different spatial extents. If one performs perturbation (or MRCI) calculations using these CASSCF MOs, the potential energy curve may be disconnected in the middle region. In fact, in the present study, we had three kinds of CASSCF solutions, namely, three MO sets. This made the potential energy curves by MCQDPT2 calculations disconnected or discontinuous.

Shepard[34] issued a warning by calling this the "multiple solution problem." In response, he proposed to adopt a state-

TABLE I. Gaussian-type basis set. *L* and "No.," respectively, denote the angular quantum number and contraction set number.

L	No.	Exponent	Coefficient
s			
	1-1	268 427.932 964 8	0.000 251 7
	1-2	40 239.416 910 5	0.001 951 1
	1-3	9 157.940 760 3	0.010 140 5
	1-4	2 592.257 513 0	0.041 148 7
	1-5	844.033 658 3	0.133 267 1
	1-6	302.585 392 4	0.313 567 7
	1-7	117.347 252 7	0.433 354 6
	1-8	46.429 408 4	0.213 394 2
	2-1	312.633 565 5	−0.023 331 9
	2-2	95.867 137 3	−0.115 224 5
	2-3	14.373 267 9	0.591 572 4
	2-4	5.828 185 3	0.496 959 8
	3-1	9.489 050 1	−0.224 689 9
	3-2	1.553 220 3	0.717 493 4
	4-1	0.627 208 3	1.000 000 0
	5-1	0.744 637 2	1.000 000 0
	6-1	0.100 948 4	1.000 000 0
	7-1	0.037 326 7	1.000 000 0
p			
	1-1	4210.392 029 2	0.000 435 6
	1-2	997.821 969 5	0.003 766 8
	1-3	323.156 125 1	0.020 202 3
	1-4	122.485 362 2	0.077 429 1
	1-5	51.150 856 3	0.211 149 5
	1-6	22.542 385 6	0.376 022 3
	1-7	10.368 623 9	0.370 218 8
	1-8	4.634 073 9	0.130 970 0
	2-1	25.644 649 4	−0.016 432 8
	2-2	3.459 806 3	0.317 978 6
	2-3	1.377 474 6	0.555 334 5
	3-1	0.518 293 3	1.000 000 0
	4-1	0.179 363 1	1.000 000 0
	5-1	0.070 805 6	1.000 000 0
	6-1	0.028 264 0	1.000 000 0
d			
	1-1	133.544 512 2	0.002 090 2
	1-2	39.792 431 1	0.016 294 6
	1-3	14.816 057 9	0.066 537 2
	1-4	6.092 877 0	0.180 904 9
	1-5	2.630 651 1	0.315 981 5
	2-1	1.125 646 8	1.000 000 0
	3-1	0.462 924 5	1.000 000 0
	4-1	0.173 438 6	1.000 000 0
f			
	1-1	12.389 659 0	1.000 000 0
	2-1	3.779 429 0	1.000 000 0
	3-1	1.359 704 0	1.000 000 0
	4-1	0.462 121 0	1.000 000 0
g			
	1-1	2.656 997 0	1.000 000 0
	2-1	0.695 741 0	1.000 000 0

averaged CASSCF approach as one of its remedies. Thus one should obtain CASSCF MOs by solving several roots in CAS-CI and averaging the density matrices produced from the respective roots. In the present study we found that it was necessary to average three roots for the $^1\Sigma_g^+$ and $^{11}\Sigma_u^+$ states.

D. Quasidegenerate perturbation theory with intruder state avoidance

The $^1\Sigma_g^+$ CASSCF wave function is composed of 21 588 CSFs. The MCQDPT2 method can treat all these configurations as the reference and can calculate their contributions to electronic correlation effects. Since the dissociation energy of the Mn dimer is expected to be small (0.1 eV), a calculation is required to this accuracy.

We use the state-averaged CASSCF method, followed by the MCQDPT2 method which was developed by Nakano.[26] The MCQDPT2 method provides an effective Hamiltonian (H^{eff}) through a perturbation expansion. When the dimension of the effective Hamiltonian is one, this is equivalent to the MRMP2 method proposed by Hirao.[35] It is known that most multireference perturbation theories are vulnerable to intruder states. In the worst case the perturbation expansion diverges. To overcome this problem, we adopt the intruder state avoidance (ISA) method proposed by Witek *et al.*[36] This ISA method has been applied to the AgH molecule[37] and gave a smooth potential energy curve. Throughout the MCQDPT2 calculations, MOs composed of 1*s*, 2*s*, and 2*p* AOs were kept frozen.

We obtain the vibrational states by solving the one-dimensional Schrödinger equation numerically using the Numerov method.[38] Potential energy values at many internuclear distances (c.a. 1500) are required for this method; we obtain them by cubic natural spline[39] (CNS) fitted to the MCQDPT2 potential energy curves.

III. RESULTS AND DISCUSSION

A. Potential energy curve

Figure 1 shows the potential energy curves of the $^1\Sigma_g^+$, $^{11}\Sigma_u^+$, and $^{11}\Pi_u$ states calculated by MCQDPT2. Figure 2 shows an enlargement of these curves between 6.0 and 6.8 a.u. It is seen that the $^1\Sigma_g^+$ state takes the lowest energy and can be considered as the ground state of the Mn dimer. Although a figure is not given, at the CASSCF level the $^1\Sigma_g^+$ and $^{11}\Sigma_u^+$ states are not bound.

For the $^1\Sigma_g^+$ state, we used three-state-averaged CASSCF MOs. For the $^{11}\Pi_u$ state, CASSCF MOs averaged between different irreps ($^{11}B_{3u}+{}^{11}B_{2u}$) were used. Use of the three-state-averaged CASSCF MOs is inferior for the lowest root than CASSCF MOs optimized purely for the lowest root. Even then the $^1\Sigma_g^+$ state is lower than the $^{11}\Pi_u$ state, so that this energy ordering should not be altered even if more elaborate calculations were performed.

Figure 1 has a shoulder near $R=3.2$ a.u. on the $^1\Sigma_g^+$ curve. This shoulder reflects the transition of the electronic configuration from ($^6S+{}^6S$) to ($^6D+{}^6D$) as the nuclear distance shortens.

The $^{11}\Sigma_u^+$ curve lies slightly above the $^1\Sigma_g^+$ curve, as shown in Fig. 2. This small energy gap is promising in predicting the experimental Heisenberg exchange coupling constant *J* (see Sec. III D).

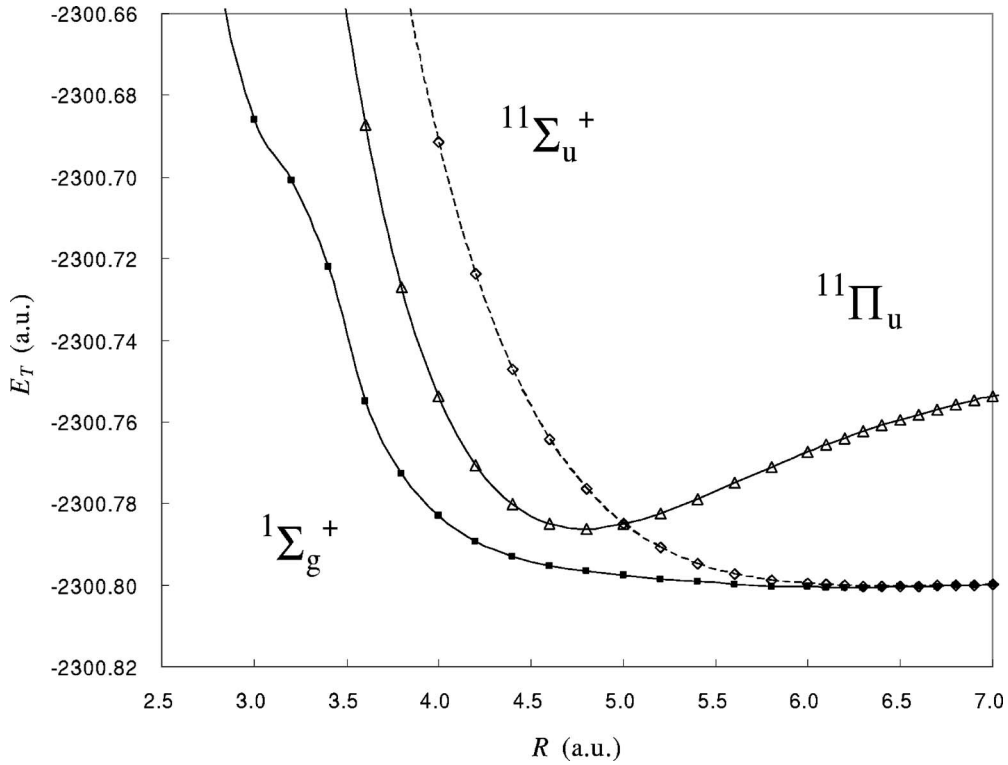

FIG. 1. Potential energy curves of the Mn dimer calculated at the MCQDPT2 level. The solid line marked by closed squares denotes the $^1\Sigma_g^+$ state. The broken line marked by white diamonds denotes the $^{11}\Sigma_u^+$ state. The solid line marked by white triangles denotes the $^{11}\Pi_u$ state.

The $^{11}\Pi_u$ curve differs from the other two states. The total energy decreases sharply around the minimum of $R=4.8$ a.u. Since the CASSCF active orbitals are composed of the $4s$ and $3d$ AOs, the electronic configuration for $^{11}\Pi_u$, due to the symmetric restriction, must approach the excited electronic configuration of $(^6S+^6D)$ as the nuclear distance increases indefinitely. It is therefore possible to test the appropriateness of the calculations by checking whether the $^{11}\Pi_u$ potential energy curve at long nuclear distances lies adequately above the ground state curve.

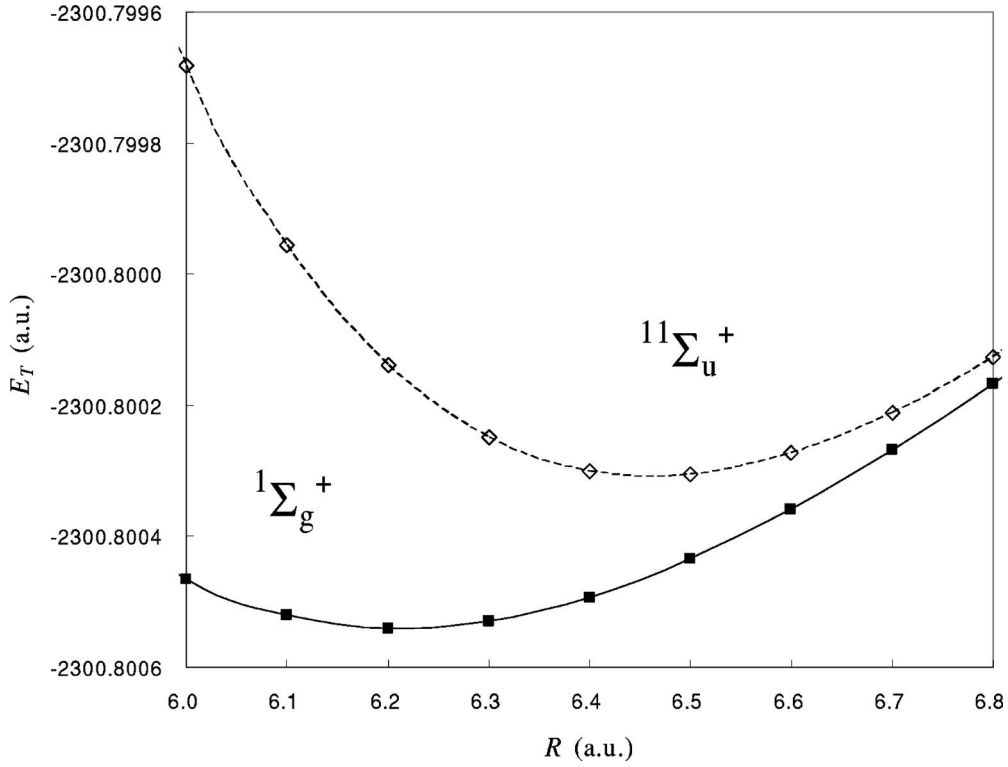

FIG. 2. Potential energy curves of the Mn dimer between 6.0 and 6.8 a.u. calculated at the MCQDPT2 level. See the caption of Fig. 1.

TABLE II. Occupation numbers in $^1\Sigma_g^+$ full-valence CI with three-state-averages CASSCF natural orbitals at $R=6.2$ a.u.

Notation in this paper	Irrep in D_{2h}	Occupation number
$4s_\sigma$	$1a_g$	2.0000
$4s^*_\sigma$	$1b_{1u}$	2.0000
$3d_{\sigma z2}$	$2a_g$	1.0321
$3d_{\pi y}$	$1b_{2u}$	1.0144
$3d_{\pi x}$	$1b_{3u}$	1.0144
$3d_{\delta x2-y2}$	$3a_g$	1.0029
$3d_{\delta xy}$	$1b_{1g}$	1.0020
$3d^*_{\delta xy}$	$1a_u$	0.9980
$3d^*_{\delta x2-y2}$	$2b_{1u}$	0.9971
$3d^*_{\pi x}$	$1b_{2g}$	0.9858
$3d^*_{\pi y}$	$1b_{3g}$	0.9858
$3d^*_{\sigma z2}$	$3b_{1u}$	0.9679

We found that the $^{11}\Sigma_g^+$ state has higher MCQDPT2 total energy than the $^{11}\Pi_u$ state from our preliminary calculations and excluded the $^{11}\Sigma_g^+$ state from the discussion here.

B. Configuration mixing

We now discuss the details of the $^1\Sigma_g^+$ wave function at $R=6.2$ a.u. Since the off-diagonal terms of the MCQDPT2 effective Hamiltonian are rather small, here we analyze the wave functions at the CASSCF level. We have performed a full-valence CI (FVCI) calculation using the three-state-averaged CASSCF natural orbitals (NOs). The characters of the NOs and their occupation numbers are listed in Table II. The $4s_\sigma$ and $4s^*_\sigma$ NOs are occupied by two electrons. The remaining ten NOs composed of the $3d$ AOs are occupied by almost a single electron. The Mulliken AO populations are 1.93 and 5.00 for the $4s$ and $3d$ AOs, indicating $(4s)^2(3d)^5\ ^6S$ for the respective atoms; $(^6S+^6S)$ is the result. This indicates that there is no strong covalent interaction between the two Mn atoms. We treat this status as van der Waals bonding in this paper. This picture is quite reasonable in view of the high $4s\rightarrow 3d$ promotion energy (2.14 eV) (Ref. 27) of the Mn atom. However, the configuration mixing in this state has a complicated feature. We cannot find any leading configurations; the maximum CI coefficient is small at 0.092 and there exist 132 configurations of which magnitude is between 0.092 and 0.05. The configuration with a coefficient 0.092 is $(4s_\sigma)^2\ (4s^*_\sigma)^2\ (3d_{\sigma z2})^2\ (3d_{\pi y})^2\ (3d_{\pi x})^2\ (3d_{\delta x2-y2})^1\ (3d_{\delta xy})^1\ (3d^*_{\delta xy})^1\ (3d^*_{\delta x2-y2})^0\ (3d^*_{\pi x})^0\ (3d^*_{\pi y})^0\ (3d^*_{\sigma z2})^1$, where we have three vacant $(3d)$ NOs. The FVCI occupation numbers for all the $3d$ AOs in Table II are, however, close to 1, giving the symbolic $^1\Sigma_g^+$ configuration as

$$(4s_\sigma)^{2.0000}(4s^*_\sigma)^{2.0000}(3d_{\sigma z2})^{1.0321}(3d_{\pi y})^{1.0144}(3d_{\pi x})^{1.0144}\times(3d_{\delta x2-y2})^{1.0029}(3d_{\delta xy})^{1.0020}(3d^*_{\delta xy})^{0.9980}(3d^*_{\delta x2-y2})^{0.9971}\times(3d^*_{\pi x})^{0.9858}(3d^*_{\pi y})^{0.9858}(3d^*_{\sigma z2})^{0.9679}. \quad (1)$$

We next look at the $^{11}\Sigma_u^+$ wave function at $R=6.4$ a.u. The symbolic $^{11}\Sigma_u^+$ configuration of the FVCI calculation with the three-state-averaged CASSCF NOs is

$$(4s_\sigma)^{2.0000}(4s^*_\sigma)^{2.0000}(3d_{\sigma z2})^{1.0000}(3d_{\pi y})^{1.0000}(3d_{\pi x})^{1.0000}\times(3d_{\delta x2-y2})^{1.0000}(3d_{\delta xy})^{1.0000}(3d^*_{\delta xy})^{1.0000}(3d^*_{\delta x2-y2})^{1.0000}\times(3d^*_{\pi x})^{1.0000}(3d^*_{\pi y})^{1.0000}(3d^*_{\sigma z2})^{1.0000}. \quad (2)$$

Unlike the $^1\Sigma_g^+$ state, there is a single dominant configuration, with coefficient 0.9999. The $(4s_\sigma)$ and $(4s^*_\sigma)$ NOs are doubly occupied, and the remaining ten NOs composed of $3d$ AOs are singly occupied. The AO populations are 1.93 and 5.00 for the $4s$ and $3d$ AOs, giving the molecular configuration of $((4s)^2(3d)^{56}S+(4s)^2(3d)^{56}S)$. From the configurations (1) and (2) we see that the $^1\Sigma_g^+$ and $^{11}\Sigma_u^+$ states by accident have almost the same the electronic configurations, although they are composed of quite different CSFs.

We now give details of the $^{11}\Pi_u$ CASSCF wave function at $R=4.8$ a.u. We have performed CSF-based FVCI calculations under the $^{11}B_{3u}$ and $^{11}B_{2u}$ symmetries, respectively, by using the canonical orbitals of the determinant-based CASSCF calculation averaged between the $(^{11}B_{3u}+^{11}B_{2u})$ states. The averaged occupation numbers of the $^{11}B_{3u}$ and $^{11}B_{2u}$ states are as follows:

$$(4s_\sigma)^{1.8943}(4s^*_\sigma)^{1.1056}(3d_{\sigma z2})^{1.000}(3d_{\pi y})^{1.4472}(3d_{\pi x})^{1.4472}\times(3d_{\delta x2-y2})^{1.000}(3d_{\delta xy})^{1.000}(3d^*_{\delta xy})^{1.000}(3d^*_{\delta x2-y2})^{1.000}\times(3d^*_{\pi x})^{1.0528}(3d^*_{\pi y})^{1.0528}(3d^*_{\sigma z2})^{1.000}. \quad (3)$$

This configuration corresponds to one-electron transfer from $(4s^*_\sigma)$ to $(3d_\pi)$ if viewed from the $^1\Sigma_g^+$ configuration. The AO populations are 1.37 for the $4s$ AO and 5.48 for the $3d$ AO, giving approximately $(4s)^{1.5}(3d)^{5.5}$. This corresponds to the molecular configuration of $(^6S+^6D)$.

We now summarize the above results. At large nuclear distance the Mn dimer is an aggregation of two Mn atoms of the ^6S ground state, and can therefore be represented by $(^6S+^6S)$. The $^{11}\Sigma_u^+$ state at the minimum of $R=6.4$ a.u. and the $^1\Sigma_g^+$ ground state at the minimum of $R=6.2$ a.u. have close correspondence with the $(^6S+^6S)$ configuration. The $^{11}\Pi_u$ state at the minimum of $R=4.8$ a.u. correlates with $(^6S+^6D)$. At distances less than 3.2 a.u., the $^1\Sigma_g^+$ ground state changes to $(^6D+^6D)$, where each Mn atom has configuration $(4s)^1(3d)^6$. Thus, as the nuclear distance decreases, the electronic configuration changes from $(^6S+^6S)$, $(^6S+^6D)$, to $(^6D+^6D)$. Electron transfer from $(4s)^2(3d)^{n-2}$ to $(4s)^1(3d)^{n-1}$ dictates the bonding. This picture has also been recognized in studies[28,29] of Sc_2 and Ti_2. The model used here can therefore be generalized to a guiding principle for analyzing the bonding mechanism of transition metal dimers.

C. Vibrational analysis

Table III lists values of ω_e and $\omega_e x_e$ derived from the ω values given by the Numerov method. For the $^1\Sigma_g^+$ state, the details of the vibrational levels are shown in Table IV. These were obtained from the vibrational levels $G(\nu)$ given by

$$G(\nu)=\omega_e(\nu+1/2)-\omega_e x_e(\nu+1/2)^2. \quad (4)$$

The ω_e and $\omega_e x_e$ values were calculated from the $G(2)$ and $G(3)$ vibrational levels. To check these values, we reversed the calculation to determine $G(\nu)$ values from the calculated

TABLE III. Bond length (R_e), dissociation energy (D_e), and vibrational frequency (ω_e) of the Mn dimer calculated at the MCQDPT2 level. The experimental values are taken from Ref. 8.

State	No. of CSF	No. of state averaged	Dimension of H^{eff}	Irrep in D_{2h}	R_e (Å) (a.u.)	D_e (eV)	ω_e (cm^{-1})	$\omega_e x_e$ (cm^{-1})
$^1\Sigma_g^+$	21 588	3	3	A_g	3.29 (6.22)	0.14[a]	53.46	0.87
$^{11}\Sigma_u^+$	12	3	3	B_{1u}	3.42 (6.46)	0.13[a]	62.64	1.36
$^{11}\Pi_u$	8	2	1	$B_{3u}+B_{2u}$	2.53 (4.79)	1.21[b]	240.47	1.30
$^1\Sigma_g^+$ (Expt.)					3.4 (6.43)	0.1	68.1	1.05

[a]Relative to $((4s)^2(3d)^5\ ^6S+(4s)^2(3d)^5\ ^6S)$.
[b]Relative to $((4s)^2(3d)^5\ ^6S+(4s)^1(3d)^6\ ^6D)$.

ω_e and $\omega_e x_e$. As shown in the columns named "Recomputed" of Table IV, the values of $G(\nu)$ emerged correctly.

We now discuss the vibrational states of the ground state. Kirkwood *et al.*[8] observed the resonance Raman spectrum of the Mn dimer in the xenon matrix and reported that the ground state is $^1\Sigma_g^+$ with $\omega_e=68.1\ \text{cm}^{-1}$ and $\omega_e x_e=1.05\ \text{cm}^{-1}$. The Numerov method for the MCQDPT2 potential energy curve gives 53.5 cm^{-1} for ω_e and 0.87 cm^{-1} for $\omega_e x_e$. Agreement between the calculated and experimental values is fairly good. The small discrepancy between the two is probably because (1) we disregard the relativistic effects which slightly shorten the bond length and (2) the Mn dimer in the matrix is compressed compared to the gaseous Mn dimer. We will discuss the relativistic effects later in Sec. III F. The calculated and experimental vibrational levels given in the third and fourth columns of Table IV show somewhat large differences because the energy in the respective levels (ν) is roughly equal to $(\nu+1/2)\omega_e$. Differences between the calculated and experimental values of $G(\nu+1)-G(\nu)$ are around 13–15 cm^{-1}, almost equal to the difference between the two ω_e's, suggesting that the Mn dimer potential in the matrix has a larger curvature.

The vibrational wave function of the $\nu=0$ level is compact, not diffuse, in contradiction to the flat potential given in Fig. 1; it has on amplitude greater than 0.01 in the range of 5.38–7.22 a.u.

Finally, we summarize the spectroscopic constants. As shown in Table III, the calculated R_e of 3.29 Å is close to the experimental value (3.4 Å) and is near the value (3.64 Å) calculated by Wang and Chen.[24] All these values of R_e, including the experimental result, are quite large compared to the values for other transition metal dimers. We calculate the dissociation energy as the total energy difference between the minimum point and the nuclear distance 100 a.u. The calculated (0.14 eV) and experimental (0.1 eV) dissociation energies are rather small. The spacing of the vibrational levels is also small. All of these results suggest that the Mn dimer is a van der Waals molecule.

D. Magnetic coupling

Yamanaka *et al.*[40] proposed the following formula (6) for evaluating the Heisenberg exchange coupling constant J_{ab} from theoretical calculations.

$$H=-2\sum_{ab} J_{ab}\boldsymbol{S}_a\cdot\boldsymbol{S}_b \tag{5}$$

$$J_{ab}=\frac{E_{\text{LS}}-E_{\text{HS}}}{\langle \boldsymbol{S}^2\rangle_{\text{HS}}-\langle \boldsymbol{S}^2\rangle_{\text{LS}}}, \tag{6}$$

where, LS and HS, respectively, designate low spin and high spin. We take E_{LS} as −2300.800 541 a.u. corresponding to

TABLE IV. Experimental and calculated vibrational levels for $^1\Sigma_g^+$. Vibrational levels of $G(\nu)$ and its spacing of $G(\nu+1)-G(\nu)$. The experimental values are taken from Ref. 8.

	Vibrational levels $G(\nu)$ (cm^{-1})			Level spacing of $G(\nu+1)-G(\nu)$ (cm^{-1})		
		Recomputed			Recomputed	
ν	Numerov	Using ω_e and $\omega_e x_e$ from Numerov	Using ω_e and $\omega_e x_e$ from Expt.	Numerov	Using ω_e and $\omega_e x_e$ from Numerov	Using ω_e and $\omega_e x_e$ from Expt.
0	26.5	26.5	33.8			
1	78.3	78.2	99.8	51.8	51.7	66.0
2	128.2	128.2	163.7	49.9	50.0	63.9
3	176.4	176.4	225.5	48.2	48.2	61.8
4	222.8	222.9	285.2	46.4	46.5	59.7
5	267.6	267.6	342.8	44.7	44.7	57.6

the $^1\Sigma_g^+$ state at $R=6.2$ bohrs, and E_{HS} as −2300.800 139 a.u. corresponding to the $^{11}\Sigma_u^+$ state at the same distance. We thereby obtain $-2.935\ \mathrm{cm}^{-1}$ for J_{ab}. However, the ESR experimentalists[6] prefer the following definition of J:

$$H = -JS_a \cdot S_b. \tag{7}$$

Thus we must double the J_{ab} value derived from the formula (5). Our calculated J value ($-5.87\ \mathrm{cm}^{-1}$) and the experimental J value ($-9\pm3\ \mathrm{cm}^{-1}$) together indicate that the Mn dimer is antiferromagnetic, so that the calculation is reasonably correct. The present result is similar to that of Wang and Chen.[24]

E. Symmetry adaptation

Previous studies based on DFT calculations gave the results in contradiction to experiment. We believe that this failure of DFT could be attributed to the following reasons. The primary reason is that the DFT method cannot evaluate van der Waals attractive force accurately. Secondly we infer that the broken-symmetry DFT approach tends to overestimate electron correlation effects, especially in the bonding region.

For the first reason, DFT would not be a good choice for studying molecular systems governed by van der Waals interactions. In such cases a new functional which accounts for dispersion forces has recently been proposed by Iikura *et al.*[41] and therefore the situation will be improved.

We now discuss limitations of the broken-symmetry approach which is now widely used in DFT calculations. In fact, a broken-symmetry spin-unrestricted DFT approach is used in Refs. 19 and 20. The broken-symmetry approach aims to account for effects arising from mixing of nearly-degenerate configurations, known as static correlation effects or multiconfigurational effects. The same approach is used also in *ab initio* MO methods such as unrestricted Hartree-Fock (UHF) and Møller-Plesset perturbation theories with UHF MOs (UMP). In the present work, for the $^{11}\Pi_u$ state, CASSCF calculations were performed by averaging the density matrices between the $^{11}B_{3u}$ and $^{11}B_{2u}$ irreps, so that the CASSCF canonical orbitals should be symmetry adapted. If the CASSCF calculations are performed under the $^{11}B_{3u}$ symmetry without averaging, the total energy decreases significantly, especially in the bonding region, and the resulting potential curve descends beneath the $^1\Sigma_g^+$ curve. The broken-symmetry CASSCF gives a fatally flawed result.

We further performed the CASSCF calculations by lowering the symmetry to C_{2h} from D_{2h}. In the case of C_{2h}, B_u, and A_g, respectively, correspond to Π_u and Σ_g^+. Both x and y components belong to B_u. At the CASSCF level, the $^{11}B_u$ state has higher energy than the ^1A_g state. However, at the MCQDPT2 level, the ^1A_g state has higher energy. Contradiction with experiment thereby arises. We found that the CASSCF electron distribution at $R=4.8$ a.u. was not symmetric with respect to x and y. Moreover, even at $R=10.0$ a.u., the total energy difference between $^{11}B_u$ and ^1A_g is 4.69 eV at the CASSCF level, but is −0.092 eV at the MCQDPT2 level. Thus the broken-symmetry calculations again give physically incorrect results.

The above discussion suggests that symmetry adaptation is critical for the CASSCF and MCQDPT2 calculations to give correct results. The broken-symmetry approach overestimates the electron correlation effects, especially in the bonding region. A similar situation may arise also in the DFT calculations.

F. Relativistic effects

In this section we consider relativistic effects on the bonding of the Mn dimer. It is known that for the first-row transition metals relativistic effects are not so large. Especially the spin-orbit interaction is expected to be small. In fact, the spin-orbit coupling is estimated to be around $200\ \mathrm{cm}^{-1}$ for the Mn dimer. Since the MCQDPT2 energy gap between the $^1\Sigma_g^+$ and $^{11}\Pi_u$ states is larger than $2000\ \mathrm{cm}^{-1}$, this energy ordering should not be altered by the spin-orbit coupling. In addition, the ordering between the $^1\Sigma_g^+$ and $^{11}\Sigma_u^+$ states should be kept because the spin-orbit coupling is zero for Σ states. Thus we consider the remaining relativistic effects (corresponding to the mass-velocity term and the Darwin term) by applying the second-order Douglas-Kroll transformation[42,43] (DK2) to the one-electron Hamiltonian within the one-component space. We treated the Mn nucleus as a point charge and used the same basis set.

The energy ordering of the four states ($^1\Sigma_g^+$, $^{11}\Sigma_u^+$, $^{11}\Pi_u$, $^{11}\Sigma_g^+$) was not altered by DK2. The $^1\Sigma_g^+$ state keeps the ground state. However, the equilibrium nuclear distance is shortened to 6.005 a.u. (3.18 Å) from 6.22 a.u. The potential energy curvature is slightly larger than the nonrelativistic one, giving D_e, ω_e, and $\omega_e x_e$ of 0.159 eV, $59.22\ \mathrm{cm}^{-1}$, and $0.95\ \mathrm{cm}^{-1}$, respectively. The calculated ω_e value becomes closer to the experimental value. The remaining difference can be ascribed to the matrix effect as stated before. The shoulder recognized near $R=3.2$ a.u. in the nonrelativistic $^1\Sigma_g^+$ potential energy curve is enlarged to a hump. The J value calculated at $R=6.0$ a.u. is $-10.9\ \mathrm{cm}^{-1}$. On the whole the bonding characteristics were not altered.

IV. CONCLUDING REMARKS

We have performed MCQDPT2 calculations for the three states ($^1\Sigma_g^+$, $^{11}\Sigma_u^+$, $^{11}\Pi_u$) of the Mn dimer, using state-averaged CASSCF MOs to obtain accurate potential energy curves. Of these three states, the $^1\Sigma_g^+$ state has the lowest energy, so we conclude that the $^1\Sigma_g^+$ state is the ground state of the Mn dimer. It follows that the Mn dimer is antiferromagnetic. The calculated bond length (3.29 Å), dissociation energy (0.14 eV), and vibrational frequency ω_e ($53.46\ \mathrm{cm}^{-1}$) agree well with the experimental values of 3.4 Å, 0.1 eV, and $66.8\ \mathrm{cm}^{-1}$. The long bond length and low vibrational frequency show that the Mn dimer is a van der Waals molecule.

ACKNOWLEDGMENT

This study was partly supported by Grants-in-Aid for Scientific Research to one of the authors (H.T.) from the Ministry of Education, Culture, Sports, Science and Technology of Japan.

[1] B. O. Roos, P. R. Taylor, and P. E. M. Siegbahn, Chem. Phys. **48**, 157 (1980).
[2] K. Andersson, P.-Å. Malmqvist, B. O. Roos, A. J. Sadlej, and K. Wolinski, J. Phys. Chem. **9**, 5483 (1990).
[3] K. Andersson, Chem. Phys. Lett. **237**, 212 (1995).
[4] H. Dachsel, R. J. Harrison, and D. A. Dixon, J. Phys. Chem. A **103**, 152 (1999).
[5] G. W. Ludwig, H. H. Woodbury, and R. O. Carlson, J. Phys. Chem. Solids **8**, 490 (1959).
[6] C. A. Baumann, R. J. Van Zee, S. V. Bhat, and W. Weltner, Jr., J. Phys. Chem. **78**, 190 (1983).
[7] K. D. Bier, T. L. Haslett, A. D. Kirkwood, and M. J. Moskovits, J. Chem. Phys. **89**, 6 (1988).
[8] A. D. Kirkwood, K. D. Bier, J. K. Thompson, T. L. Haslett, A. S. Huber, and M. Moskovits, J. Phys. Chem. **95**, 2644 (1991).
[9] A. Kant, S. Lin, and B. Strauss, J. Chem. Phys. **49**, 1983 (1968).
[10] J. R. Lombardi and B. Davis, Chem. Rev. (Washington, D.C.) **102**, 2431 (2002).
[11] R. K. Nesbet, Phys. Rev. **135**, A460 (1964).
[12] J. Harris and R. O. Jones, J. Chem. Phys. **70**, 830 (1979).
[13] N. Fujima and T. Yamaguchi, J. Phys. Soc. Jpn. **64**, 1251 (1995).
[14] S. K. Nayak and P. Jena, Chem. Phys. Lett. **289**, 473 (1998).
[15] S. K. Nayak, B. K. Rao, and P. Jena, J. Phys. C **10**, 10863 (1998).
[16] M. R. Pederson, F. Reuse, and S. N. Khanna, Phys. Rev. B **58**, 5632 (1998).
[17] N. Desmarais, F. A. Reuse, and S. N. Khanna, J. Chem. Phys. **112**, 5576 (2000).
[18] S. Yanagisawa, T. Tsuneda, and K. Hirao, J. Chem. Phys. **112**, 545 (2000).
[19] C. J. Barden, J. C. Rienstra-Kiracofe, and H. F. Schaefer III, J. Chem. Phys. **113**, 690 (2000).
[20] G. L. Gutsev and C. W. Bauschlicher, Jr., J. Phys. Chem. A **107**, 4755 (2003).
[21] M. Valiev, E. J. Bylaska, and J. H. Weare, J. Chem. Phys. **119**, 5955 (2003).
[22] P. Bobadova-Parvanova, K. A. Jackson, S. Srinivas, and M. Horoi, J. Chem. Phys. **122**, 014310 (2005).
[23] C. W. Bauschlicher, Jr., Chem. Phys. Lett. **156**, 95 (1989).
[24] B. Wang and Z. Chen, Chem. Phys. Lett. **387**, 395 (2004).
[25] P. Celani and H.-J. Werner, J. Chem. Phys. **112**, 5546 (2000).
[26] H. Nakano, J. Chem. Phys. **99**, 7983 (1993).
[27] C. E. Moore, *Ionization Potential and Ionization Limits from the Analysis of Optical Spectra*, Natl Bur. Stand. Ref. Data Ser., Natl Bur. Stand. (U.S.) Circ. No. 34 (U.S. GPO, Washington, DC, 1970).
[28] Y. Suzuki, S. Asai, K. Kobayashi, T. Noro, F. Sasaki, and H. Tatewaki, Chem. Phys. Lett. **268**, 213 (1997).
[29] Y. Suzuki, T. Noro, F. Sasaki, and H. Tatewaki, THEOCHEM **461–462**, 351 (1999).
[30] T. Koga, H. Tatewaki, H. Matsuyama, and Y. Satoh, Theor. Chem. Acc. **102**, 105 (1999); see also http://www.nsc.nagoya-cu.ac.jp/~htatewak/CGTF/8433.843.8.txt
[31] H. Tatewaki, T. Koga, and S. Yamamoto, Theor. Chem. Acc. **105**, 55 (2000); see also http://www.nsc.nagoya-cu.ac.jp/~htatewak/POL/pol7433.743.7.txt
[32] M. Sekiya, T. Noro, Y. Osanai, and T. Koga, Theor. Chem. Acc. **106**, 297 (2001); see also http://setani.sci.hokudai.ac.jp/qc/basis/html/mn.html
[33] GAMESS, Version 10, November 2004; M. W. Schmidt, K. K. Baldridge, J. A. Boatz *et al.*, J. Comput. Chem. **14**, 1347 (1993).
[34] R. Shepard, in *Relativistic and Electron Correlation Effects in Molecules and Solids*, edited by G. L. Malli (Plenum, New York, 1994), pp. 161–177.
[35] K. Hirao, Chem. Phys. Lett. **190**, 374 (1992).
[36] H. A. Witek, Y.-K. Choe, J. P. Finley, and K. Hirao, J. Comput. Chem. **23**, 957 (2002).
[37] H. A. Witek, D. G. Fedorov, K. Hirao, A. Viel, and P.-O. Widmark, J. Chem. Phys. **116**, 8396 (2002).
[38] J. M. Thijssen, *Computational Physics* (Cambridge University Press, Cambridge, 1999).
[39] A. Ralston and P. Rabinowitz, *A First Course in Numerical Analysis*, 2nd ed. (McGraw-Hill, New York, 1978).
[40] S. Yamanaka, R. Takeda, and K. Yamaguchi, Polyhedron **22**, 2013 (2003).
[41] H. Iikura, T. Tsuneda, T. Yanai, and K. Hirao, J. Chem. Phys. **115**, 3540 (2001).
[42] M. Douglas and N. M. Kroll, Ann. Phys. (N.Y.) **82**, 89 (1974).
[43] B. A. Hess, Phys. Rev. A **33**, 3742 (1986).